

Universal Adversarial Perturbations and Image Spam Classifiers

Andy Phung* Mark Stamp†,§

Abstract

As the name suggests, image spam is spam email that has been embedded in an image. Image spam was developed in an effort to evade text-based filters. Modern deep learning-based classifiers perform well in detecting typical image spam that is seen in the wild. In this chapter, we evaluate numerous adversarial techniques for the purpose of attacking deep learning-based image spam classifiers. Of the techniques tested, we find that universal perturbation performs best. Using universal adversarial perturbations, we propose and analyze a new transformation-based adversarial attack that enables us to create tailored “natural perturbations” in image spam. The resulting spam images benefit from both the presence of concentrated natural features and a universal adversarial perturbation. We show that the proposed technique outperforms existing adversarial attacks in terms of accuracy reduction, computation time per example, and perturbation distance. We apply our technique to create a dataset of adversarial spam images, which can serve as a challenge dataset for future research in image spam detection.

1 Introduction

E-mail, or electronic mail, is one of the most popular forms of communication in the world, with over 3.9 billion active email users [4]. As a side effect of this rapid growth, the number of unwanted bulk email messages—i.e., spam messages—sent with commercial or malicious intent has also grown. According to [4], 60 billion spam emails will be sent each day for the next three years.

While text-based spam filtering systems are in use by most, if not all, e-mail clients [8], spammers can embed messages in attached images to evade such systems—such messages are known as image spam. Image spam detectors based on optical character recognition (OCR) have been deployed to combat such e-mail. As a countermeasure, spammers can modify images so as to disrupt OCR based techniques [9].

In recent years, deep learning models, such as multi-layer perceptrons and convolutional neural networks, have been successfully applied to the image spam problem [9, 2, 25, 6, 12, 1, 24]. Note that these techniques do not rely on OCR, but instead detect image spam directly, based on characteristics of the images.

With the recent development of perturbation methods, the possibility exists for spammers to utilize adversarial techniques to defeat image-based machine learning detectors [26]. To date, we are not aware of perturbation techniques having been used by image spammers, but it is highly likely that this will occur in the near future.

The main contributions of our research are the following.

- We show that the universal perturbation adversarial attack is best suited for the task of bypassing deep learning-based image spam filters.
- We propose a new image transformation-based attack that utilizes the maximization of layer activations to produce spam images containing universal perturbations. This technique focuses perturbations in the most salient regions, as well as concentrating natural features in the remaining regions.
- We compare our proposed adversarial technique to existing attacks and find that our approach outperforms all others in terms of accuracy reduction, computation time per example, and perturbation magnitude.
- We generate a large dataset containing both non-spam and adversarial spam images using our proposed attack. The authors will make this dataset available to researchers.

The remainder of this chapter is organized as follows. In Section 2, we provide an overview of relevant research and related work. In Section 3, we evaluate adversarial attacks in the context of image spam, and in Section 4, we present our proposed attack. Finally, Section 5 concludes this chapter, where we have included suggestions for future work.

*phungandy0080@students.esuhsd.org

†mark.stamp@sjsu.edu

§Department of Computer Science, San Jose State University, San Jose, California

2 Background

2.1 Image Spam Filtering

The initial defenses against image spam relied on optical character recognition (OCR). In such OCR-based systems, text is extracted from an image, at which point a traditional text-based spam filter can be used [3]. As a reaction to OCR-based techniques, spammers introduced images with slight modifications, such as overlaying a light background of random artifacts on images, which are sufficient to render OCR ineffective. The rise of learning algorithms, however, has enabled the creation of image spam filtering systems based directly on image features.

In 2008, a filtering system using a global image feature-based probabilistic boosting tree was proposed, and achieved an 89.44% detection rate with a false positive rate of 0.86% [9]. Two years later, an artificial neural network for image classification was proposed [25]. These latter authors used were able to classify image spam with 92.82% accuracy based on color histograms, and 89.39% accuracy based on image composition extraction.

The two image spam detection methods presented in [2] rely on principal component analysis (PCA) and support vector machines (SVM). In addition, the authors of [2] introduce a new dataset that their methods cannot reliably detect. Two years later, the authors of [6] improved on the results in [2] by training a linear SVM on 38 image features, achieving 98% accuracy in the best case. The authors also introduce a challenge dataset that is even more challenging than the analogous dataset presented in [2].

The recent rise of deep learning, a subfield of machine learning, coupled with advances in computational speed has enabled the creation of filtering systems capable of considering not only image features, but entire images at once. In particular, convolutional neural networks (CNN) are well suited to computer vision tasks due to their powerful feature extraction capabilities.

In recent years, CNNs have been applied to the task of image spam detection. For example, in [1] a CNN is trained on an augmented dataset of spam images, achieving a 6% improvement in accuracy, as compared to previous work. Similarly, the authors of [12] consider a CNN, which achieved 91.7% accuracy. In [24], a CNN-based system is proposed, which achieves an accuracy of 99% on a real-world image spam dataset, 83% accuracy on the challenge dataset in [2] (an improvement over previous works), and 68% on the challenge dataset in [6].

From the challenge datasets introduced in [2] and [6], we see that the accuracy of machine learning-based filtering systems can be reduced significantly with appropriate modifications to spam images. In this research, we show that the accuracy of such systems can be reduced far more by using the adversarial learning approach that we present below.

2.2 Adversarial Learning

The authors of [26] found that by applying an imperceptible filter to an image, a given neural network’s prediction can be arbitrarily changed. This filter can be generated from the optimization problem

$$\begin{aligned} & \text{minimize } \|r\|_2 \\ & \text{subject to } f(x+r) = l \text{ and } x+r \in [0, 1]^m \end{aligned}$$

where f is the classifier, r is the minimizer, l is the target label, and m is the dimension of the image. The resulting modified images are said to be *adversarial examples*, and the attack presented in [26] is known as the *L-BFGS Attack*. These adversarial examples generalize well to different network architectures and networks.

More recently, many advances have been made in both adversarial example generation and detection. For example, in [28] a taxonomy is proposed for generation and detection methods, as well as a threat model. Based on this threat model, the task of attacking neural network-based image spam detectors requires an attack that is false-negative (i.e. generative of positive samples misclassified as negative) and black-box (i.e. the attacker does not have access to the trained model). Attacks on image spam classifiers must satisfy these two criteria.

After the introduction of the L-BFGS Attack, the authors of [10] built on their work in [26] by introducing the *Fast Gradient Sign Method* (FGSM). This method uses the gradient of the loss function with respect to a given input image to efficiently create a new image that maximizes the loss, via backpropagation. This can be summarized with the expression

$$\text{adv}_x = x + \epsilon \text{sign}(\nabla_x J(\theta, x, y))$$

where θ is the parameters of the model, x is the input image, y is the target label, and J is the cost function used to train the model. These authors also introduce the notion that adversarial examples result from linear behavior in high-dimensional spaces.

The authors of [5] introduce *C&W’s Attack*, a method designed to combat *defensive distillation*, which consists of training a pair of models such that there is a low probability of successively attacking both models. C&W’s Attack is a non-box constrained variant of the L-BFGS Attack that is more easily optimized and effective against both distilled and undistilled networks. They formulate adversarial example generation as the optimization problem

$$\begin{aligned} & \text{minimize } D(x, x + \delta) + c \cdot f(x + \delta) \\ & \text{such that } x + \delta \in [0, 1]^n \end{aligned}$$

where x is the image, D is one of the three distance metrics described below, and c is a suitably chosen constraint (the authors choose c with binary search). The authors also utilize three distance metrics for measuring perturbation: L_0 (the number of altered pixels), L_2 (the Euclidean distance), and L_∞ (the maximum change to any of the coordinates), and introduced three subvariants of their attack that aim to minimize each of these distance metrics.

It is important to note that the previously mentioned attacks require knowledge of the classifier’s gradient and, as such, cannot be directly deployed in a black-box attack. In [19], the authors propose using a surrogate model for adversarial example generation to enable the transferability of adversarial examples to attack black-box models. Differing from gradient-based methods, the authors of [7] introduced a method, *Zeroth Order Optimization (ZOO)*, which is inspired by the work in [5]. The ZOO technique employs gradient estimation, with the most significant downside being that it is computationally expensive.

The paper [14] introduces the *DeepFool* attack, which aims to find the minimum distance from the original input images to the decision boundary for adversarial examples. They found that the minimal perturbation needed for an affine classifier is the distance to the separating affine hyperplane, which is expressed (for differentiable binary classifiers) as

$$\begin{aligned} & \text{argmin}_{\eta_i} \|\eta_i\|_2 \\ & \text{such that } f(x_i) + \nabla f(x_i)^T \eta_i = 0 \end{aligned}$$

where i denotes the iteration, η is the perturbation, and f is the classifier. In comparison to FGSM, DeepFool minimizes the magnitude of the perturbation, instead of the number of selected features. This would appear to be ideal for spammers, since it would tend to minimize the effect on an image.

The *universal perturbation* attack presented in [13] is also suited to the task at hand. We believe that universal adversarial examples are most likely to be deployed by spammers against black-box models due to their simplicity and their transferability across architectures. Generating universal perturbations is an iterative process, as the goal is to find a vector v that satisfies

$$\|v\|_p \leq \xi \quad \text{and} \quad \mathbb{P}_{x \sim \mu}(\hat{k}(x + v) \neq \hat{k}(x)) \geq 1 - \delta$$

where μ is a distribution of images, \hat{k} is a classification function that outputs for each image x and a label $\hat{k}(x)$. The results in [13] show that universal perturbations are misclassified with high probability, suggesting that the existence of such perturbations are correlated to certain regions of the decision boundary of a deep neural network.

Finally, the authors of [11] propose input restoration with a preprocessing network to defend against adversarial attacks. The authors’ defense improved the classification precision of a CNN from 10.2% to 81.8%, on average. These results outperform existing input transformation-based defenses.

3 Evaluating Adversarial Attacks

3.1 Experimental Design

The two multi-layer perceptron and convolutional neural network architectures presented in [24] are each trained on both of the dataset presented in [9], which henceforth will be referred to as the *ISH Dataset*, and the dataset presented in [6], which henceforth will be referred to as the *MD Dataset* (modified Dredze). We use TensorFlow [27] to train our models—both architectures have been trained as they were presented in their respective articles on each of the datasets. NumPy [17] and OpenCV [18] are used for numerical operations and image processing tasks, respectively. All computation are performed on a laptop with 8GB ram, using Google Colaboratory’s Pro GPU.

The ISH Dataset contains 928 spam images and 830 non-spam images, while the MD Dataset contains 810 spam images and 784 non-spam images; all images in both datasets are in *jpg* format. These datasets are summarized in Table 1.

Table 1: Image spam datasets

Name	Spam images	Non-spam images
ISH dataset	928	830
MD dataset	810	784
Total	1738	1613

Dataset preprocessing for the networks presented in [24] consist of downsizing each of the images such that their dimensions are 32×3 , applying zero-parameter Canny edge detection [20] to a copy of the downsized image, and concatenating the downsized image with the copy that had Canny edge detection applied. This process results in 64 images, which are used to train the two neural networks, one for the ISH dataset, and one for the MD dataset. The four resulting models achieved accuracies within roughly 7% of the accuracies reported in [24].

To enable the generation of adversarial examples, four larger models with an input size of 400x400 are also trained on the original datasets. The first few layers of each of these models are simply used to downscale input images such that the original architectures can be used after downscaling. These four alternative models achieve accuracy roughly equivalent to the original models. The four adversarial attacks (FGSM, C&W’s Attack, DeepFool, and Universal Perturbation) utilize these four alternative models to generate adversarial examples that can then be formatted as the original datasets to attack the original four models. This procedure attempts to exploit the transferability of adversarial examples to similar architectures.

The IBM Adversarial Robustness Toolbox (ART) [16] is used to implement C&W’s Attack, DeepFool, and Universal Perturbations, while FGSM was implemented independently from scratch. An attempt was made to optimize the parameters of each technique—the resulting parameters are summarized in Table 2. Note that for the Universal Perturbation attack, FGSM was used as the base attack, as the IBM ART allows any adversarial attack to be used for computing universal perturbations.

Table 2: Attack parameters

Attack	Description	Value
FGSM	perturbation magnitude	0.1
C&W’s attack	target confidence	0
	learning rate	0.001
	binary search steps	20
	maximum iterations	250
	initial trade-off	100
DeepFool	batch size	1
	max iterations	500
	overshoot parameter	10^{-6}
	class gradients	10
Universal Perturbation	batch size	1
	target accuracy	0%
	max iterations	250
	step size	64
	norm	∞

The metrics used to evaluate each of the four attacks are the average accuracy, area under the curve (AUC) of the receiver operating characteristic (ROC) curve, average L_2 perturbation

measurement (Euclidean distance), and average computation time per example for each of the four models. Scikit-learn [21] was used to generate the ROC curves for each attack.

We use 251 data points for accuracy and L_2 distances collected for the FGSM, DeepFool, and Universal Perturbation experiments, in accordance with the full size of the test dataset, which contains 251 examples for generating adversarial examples. However, only 28 data points were collected from the C&W’s Attack experiment due to the large amount of time required to generate each data point (roughly five minutes per data point). The technique that will be used as the basis of our proposed attack will be selected based on the performance of each attack, as presented in the next section.

3.2 Analysis

The mean accuracy, computation time per example, and L_2 distance were recorded for each of the four models attacked by each of the attack methods. This data was compiled into the tables discussed in this section.

From Table 3 we see that for FGSM, the accuracy of the attacked models is shown to vary inconsistently while Figure 1 shows that the distribution of the L_2 distances of the generated adversarial examples skew right. Based on these results and corresponding density plots of the accuracy and L_2 distance distributions, the FGSM attack can be ruled out as a candidate due to poor accuracy.

Table 3: Mean accuracy per adversarial example

Model	FGSM	C&W’s Attack	DeepFool	Universal Perturbation
MLP (ISH)	95.2%	89.2%	98.8%	98.7%
CNN (ISH)	36.2%	49.6%	61.5%	49.9%
MLP (MD)	69.7%	75.6%	93.5%	94.3%
CNN (MD)	82.8%	77.2%	14.5%	8.4%

The mean L_2 (Euclidean) distances of the adversarial examples are given in Table 4. The distribution of distances appears to be roughly equivalent across all attacks.

Table 4: Mean L_2 (Euclidean) distance of adversarial examples from original images

Model	FGSM	C&W’s Attack	DeepFool	Universal Perturbation
MLP (ISH)	11537.55	10321.77	11513.26	11483.72
CNN (ISH)	11108.44	10924.14	11216.19	11416.58
MLP (MD)	8998.71	9185.04	9566.02	9490.56
CNN (MD)	9144.49	9009.91	9128.99	9381.15

DeepFool can also be ruled as a candidate, as the attack has been seen to be only marginally better than the FGSM attack in terms of performance, while also having a significantly higher average computation time per adversarial example. This can be observed in Table 5, where the computation time per example varies greatly.

Table 5: Mean computation time per adversarial example

Model	FGSM	C&W’s Attack	DeepFool	Universal Perturbation
MLP (ISH)	0.180	269.65	19.90	4.37
CNN (ISH)	0.038	251.01	4.75	2.87
MLP (MD)	0.164	270.58	36.30	3.71
CNN (MD)	0.165	244.47	1.48	5.23

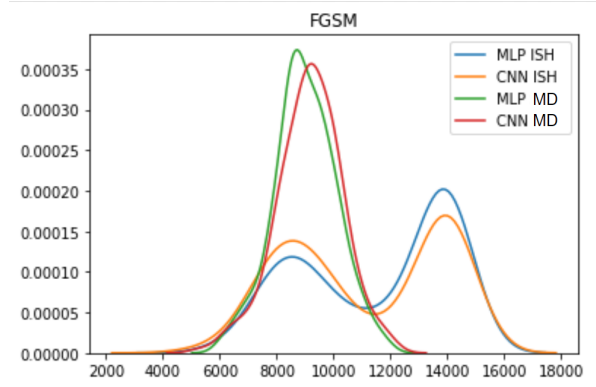


Figure 1: Density plot of L_2 (Euclidean) distances (Fast Gradient Sign Method)

In contrast, C&W’s Attack shows consistent performance in all three metrics at the cost of high computation time (roughly five minutes per adversarial example). The consistency of this attack is ideal from a spammer’s perspective, though the trade-off is a relatively high computation time. In addition, the left skew of this attack with respect to L_2 distance, as presented in Figure 2, indicates that the perturbation made to spam images is much lower in comparison to the other attacks.

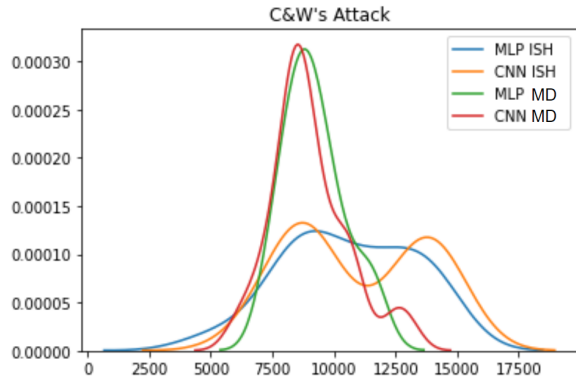


Figure 2: Density plot of L_2 (Euclidean) distances (C&W’s Attack)

The Universal Perturbation attack is inconsistent in terms of accuracy, as shown in Table 3 where the mean accuracy across the four models is clearly shown to fluctuate wildly, but this is simply due to the fact that only one perturbation (albeit with varying success across architectures) is applied to all spam images, which is highly advantageous for spammers. The generation and application of this perturbation to an image takes roughly four seconds, which would result in greater performance in a real-world spam setting in comparison to C&W’s Attack.

To further compare C&W’s Attack and the Universal Perturbation attack, the ROC curves of the two are presented in Figure 3. These ROC curves can be used to quantify the diagnostic ability of the models attacked by each method.

The ROC curve for C&W’s attack is much noisier due to being generated from only 28 data points. Taking this into consideration, it can be inferred that both C&W’s Attack and the Universal Perturbation attack are able to reduce the areas under the ROC curve (AUC) of the attacked models to values close to 0.5. This suggests that both attacks are able to reduce the class separation capacity of attacked image spam classifiers to essentially random.

To analyze the differences in distribution of the accuracy and L_2 distance data collected from the trials conducted on C&W’s Attack and the Universal Perturbation attack, the Mann-Whitney U Test was utilized via its implementation in SciPy [22]. The Mann-Whitney U Test compares two populations—in this case, the accuracy and L_2 distance data from both attacks for each attacked model. The null hypothesis (H_0) for the test is that the probability is 50% that a randomly drawn value from the first population will exceed a value from the second population. The result of each test is a Mann-Whitney U Statistic (not relevant in our case) and a p -value. We use the p -value to determine whether the difference between the data is statistically significant, where the standard

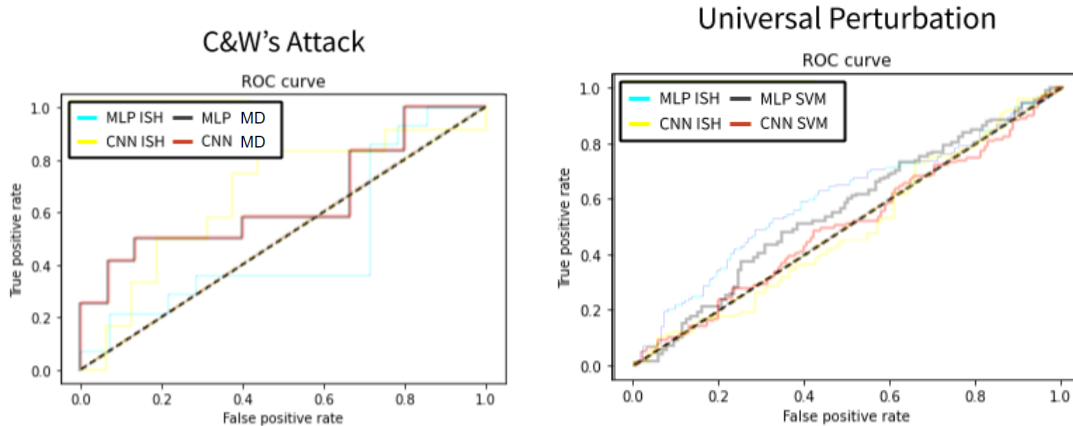


Figure 3: ROC curves of C&W’s Attack and the Universal Perturbation when used to attack the four classifiers

threshold is $p = 0.05$. The results of these tests are given in Table 6.

Table 6: Mann-Whitney U Test results comparing C&W’s Attack and the Universal Perturbation attack

Model	Accuracy p -value	L_2 distance p -value
MLP ISH	0.000 (H0 is rejected)	0.034 (H0 is rejected)
CNN ISH	0.384 (H0 is not rejected)	0.098 (H0 is not rejected)
MLP MD	0.000 (H0 is rejected)	0.057 (H0 is not rejected)
CNN MD	0.000 (H0 is rejected)	0.016 (H0 is rejected)

The results in Table 6 imply that the performance of these two attacks (C&W’s Attack and the Universal Perturbation attack) are nearly identical when attacking a CNN trained on the ISH dataset, as evidenced in the second row, where the null hypothesis is not rejected. However, the L_2 distance measurement for spam images that have had the universal perturbation applied should remain constant relative to the original spam image. Therefore, the results of these tests suggest that the Universal Perturbation attack is able to achieve similar performance to C&W’s Attack, in terms of perturbation magnitude, with a much lower computation time per example in comparison to C&W’s Attack.

Given the above evidence, the Universal Perturbation attack is the best choice for image spam, as it is unrivaled in terms of potential performance in a real-world setting. The key advantages of the Universal Perturbation attack include that it generates a single perturbation to be applied to all spam images, and its relatively fast computation time per adversarial example. Therefore, Universal Perturbation will be used as a basis for our image transformation technique, as discussed and analyzed in the remainder of this paper. A sample adversarial spam image generated with the Universal Perturbation attack is presented in Figure 4.

4 Inceptionism-Augmented Universal Perturbations

4.1 Procedure

Based on the results and discussion above, a transformation that is applied to spam images prior to generating adversarial examples, since perturbations cannot be transformed after application, should meet the following conditions.

- Lower the misclassification rate
- Preserve adversarial effects after image resizing
- Make non-spam features more prominent, while retaining legibility

Given the above criteria, a reasonable approach would be to maximize the presence of “natural features” in a given spam image. That is, the features characteristic of non-spam images learned by classifiers should be maximized whilst retaining legibility. To accomplish this, the procedure for



Figure 4: Adversarial spam image generated with the Universal Perturbation attack

maximizing the activation of a given output neuron (in this case, the non-spam output neuron), as introduced in [15], dubbed "DeepDream", can be used to increase the number of natural features in all images from the non-spam subsets of the ISH and MD datasets. This is accomplished by maximizing the activations of the convolutional layer with the greatest number of parameters and output layer in the corresponding CNNs. The resulting two sets of images that have had DeepDream applied ("dreamified" images) are then grouped into batches of four images. The weighted average of the four images in each batch can then be taken to produce two processed non-spam datasets of images with high concentrations of natural features, as batches of greater than four images may result in high noise. Each of the images in the resulting two non-spam datasets are henceforth referred to as *natural perturbations*.

To preserve the adversarial effect that the universal perturbation introduces, the Gradient-weighted Class Activation Mapping (Grad-CAM) technique introduced in [23] is used to generate a class activation map for each spam image in each dataset. The inverse of each such map is used with a natural perturbation generated from the same dataset to remove the regions of the natural perturbation where the class activation map is highest. By superimposing the resulting natural perturbations onto the corresponding spam images, the regions where the universal perturbation is most effective are left intact while the regions of the spam images affected by the natural perturbations benefit by being more non-spam-like. The presence of natural features in the resulting spam images should also result in robustness against resizing prior to inference by a deep learning-based image spam detection model, as the natural features should be still be somewhat preserved even after being shrunken.

The universal perturbation is then applied to each of the resulting spam images. The result is that we potentially reduce a deep learning-based image spam detector's accuracy due to the presence of a natural perturbation and a universal adversarial perturbation and retain some sort of adversarial effect in the case of resizing. This procedure also allows for the retention of legible text within spam images.

4.2 Implementation

To generate our two sets of "dreamified" images, the CNN architecture presented in [24] is trained on both the ISH and MD datasets, with inverted labels to allow for the maximization of the activations of the neurons corresponding to non-spam images, as the activations for spam images would be maximized if the labels weren't inverted. These two models are trained with the TensorFlow Keras API, with the hyperparameters given in [24]. For each of the models, the convolutional layer with the highest number of parameters and the output layer were chosen as the layers in which the activation should be maximized via gradient ascent, as the aforementioned convolutional layer is responsible for recognizing the most complex natural features. Each of the images from the non-spam subsets of

the ISH and MD datasets were used for inference on the two CNN models. The CNN models use the losses of the chosen layers to iteratively update the non-spam images with gradient ascent so that the number of non-spam features is maximized. Each non-spam image is updated for 64 iterations with an update size of 0.001. The resulting “dreamified” images are then grouped into batches of 4 and blended via evenly distributed weighted addition to produce a total of 392 grayscale images, each of size $400 \times 400 \times 1$. These 392 grayscale images are evenly split between the ISH dataset and MD datasets.

To utilize GradCAM, the CNN architecture presented in [24] is trained on both the ISH and MD datasets with normal labels. For each image from the spam subsets of the ISH and MD datasets, GradCAM is used to generate a corresponding class activation map based on the activations of the last convolutional layer in each of the two models. This is accomplished by computing the gradient of the top predicted class with respect to the output feature map of the last convolutional layer, using the mean intensity of the gradient over specific feature map channels. OpenCV [18] is then used to upscale each of the class activation maps to 400×400 , convert them to binary format, and invert the result to allow the class activation maps to be applied to the natural perturbations such that only the areas with highest activation will contain the natural perturbations. The bitwise AND of each processed class activation map and a randomly selected natural perturbation can then be used to generate two sets of processed natural perturbations, which are superimposed on the corresponding spam images from each of the two spam subsets. This procedure results in two subsets of spam images with natural perturbations.

Lastly, the universal perturbation is generated and applied to all images within the two spam image subsets that have had natural perturbations applied. For this operation, we use the IBM Adversarial Robustness Toolbox [16]. The hyperparameters for the Universal Perturbation attack remain the same as those given in Table 2, above.

4.3 Performance Evaluation

The mean accuracy, computation time per example, and L_2 distance were recorded for each of the four models attacked using spam images with modified universal perturbations. This is analogous to what was done during the attack selection process. This data has been compiled into the tables discussed in this section.

As can be seen from the results in Table 7, the proposed method for generating adversarial spam images is capable of lowering a learning-based model’s accuracy to 23.7%. In addition, on average, our proposed technique is much more effective while being evenly distributed in terms of accuracy on similar learning-based models.

Table 7: Mean accuracy of each model with spam images created by the proposed method

Images	MLP (ISH)	CNN (ISH)	MLP (MD)	CNN (MD)
Modified spam images	80.1%	98.8%	98.4%	75.3%
Modified spam images with Universal Perturbations	72.2%	50.4%	78.7%	23.7%

From Table 8, we see that in contrast to C&W’s Attack, which on average takes 258.93 seconds per example, the time necessary to generate adversarial spam images with natural perturbations is significantly lower and comparable to that of the original Universal Perturbation attack. This is another advantage of our proposed attack.

Table 8: Mean computation time per adversarial spam image (in seconds)

MLP (ISH)	CNN (ISH)	MLP (MD)	CNN (MD)
5.46	5.15	5.87	4.80

The mean L_2 distances and the distribution of the L_2 distances of the modified adversarial spam images are given in Table 9. From Figure 5, we see that the distributions of these distances are, on average, not skewed, indicating that the natural perturbations have had a slight negative effect on the spam image L_2 distances, as the distributions for the original Universal Perturbation attack were skewed to the left.

Table 9: Mean L_2 (Euclidean) distance of modified adversarial spam images from original images

MLP (ISH)	CNN (ISH)	MLP (MD)	CNN (MD)
11392.02	11309.40	9440.69	9628.61

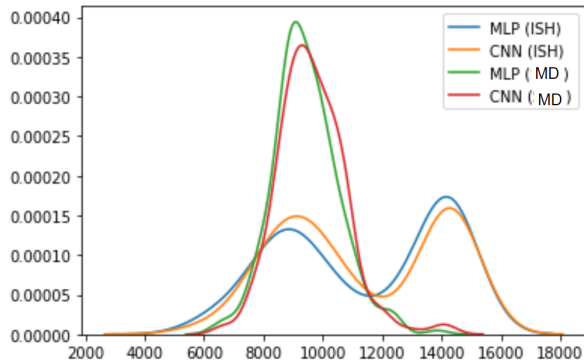


Figure 5: Density plot of L_2 (Euclidean) distances of the modified adversarial spam images from the original images

The ROC curves of the models attacked by the proposed method, which appear in Figure 6, are slightly worse in comparison to that of the original Universal Perturbation attack, suggesting once more that the attack is capable of reducing the class separation capacity of attacked image spam classifiers to essentially random.

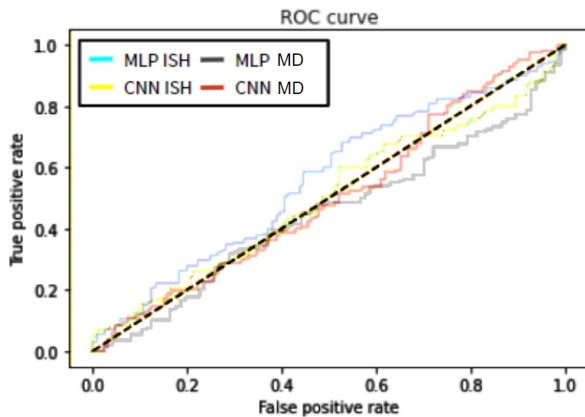


Figure 6: ROC curves of each of the four models attacked by the modified spam images generated with the proposed method

4.4 Proposed Dataset Analysis

Figure 7 contains an example of a modified adversarial spam images. From this image, we observe that the proposed method was able to effectively utilize class activation maps generated with GradCAM to selectively apply a random natural perturbation to the spam image. As discussed in the previous section, this decreases classification accuracy even prior to the application of a universal perturbation.

To fully evaluate the effect of the modified adversarial spam images from the two modified datasets, two sets of class activation maps are generated from the spam subsets of the two datasets using GradCAM and the corresponding CNN models. These activation maps are then averaged to obtain two heatmaps from the class activation maps, as shown in Figures 10 and 11. For comparison, the same process was applied to the original datasets to obtain Figures 8 and 9.

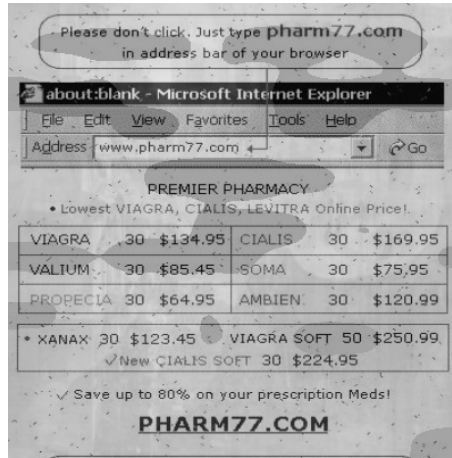


Figure 7: Example of modified adversarial spam image generated with the proposed method

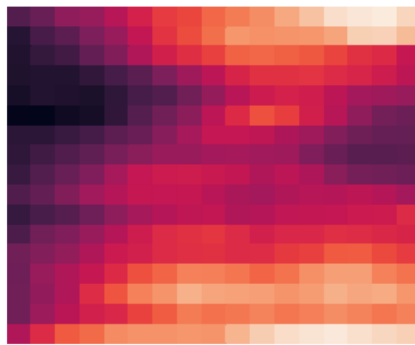


Figure 8: ISH spam data

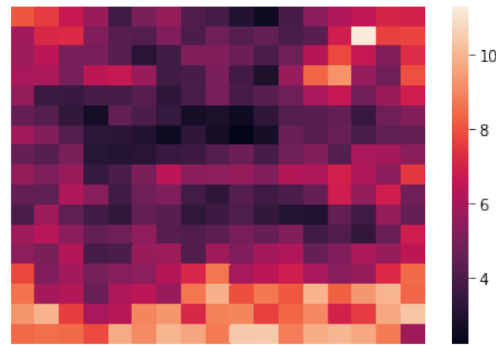


Figure 9: MD spam data

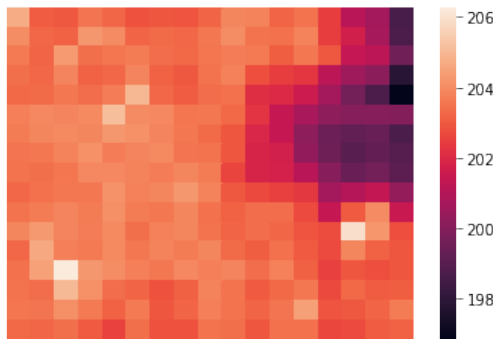


Figure 10: Modified ISH spam data

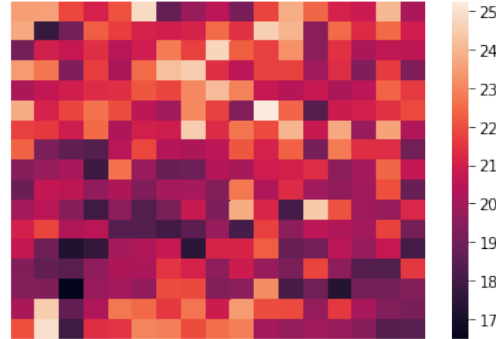


Figure 11: Modified MD spam data

As can be seen in Figures 8 and 9, the activation regions for spam images from the original ISH and MD datasets are skewed towards the top and bottom. The narrow shape of these regions represent the regions in spam images that generate the highest activations in the neurons of the deep learning-based classifier. The central region of the average class activation map for spam images from the MD dataset is much darker in comparison to that of spam images from the ISH dataset due to the superimposition of natural images directly onto spam features, as described in [6].

In contrast, Figures 10 and 11 indicate that the introduction of natural and universal adversarial perturbations are able to more evenly distribute the activation regions. This result shows that the spam images from the modified datasets are much closer—in terms of natural features—to non-spam images. This also suggests that the proposed method outperforms the procedure used to generate the original MD dataset as outlined in [6].

5 Conclusion and Future Work

Modern deep learning-based image spam classifiers can accurately classify image spam that has appeared to date in the wild. However, spammers are constantly creating new countermeasures to defeat anti-spam technology. Consequently, the eventual use of adversarial examples to combat deep learning-based image spam filters is inevitable.

In this chapter, four adversarial attacks were selected based on specific restrictions and constraints of the image spam problem. These adversarial attacks were evaluated on the CNN and MLP architectures introduced in [24]. For training data, we used the dataset presented in [9] and [6]. The Fast Gradient Sign Method (FGSM) attack, C&W’s Attack, DeepFool, and the Universal Perturbation attack were all evaluated based on mean accuracy reduction, mean computation time per adversarial spam image, mean L_2 distance from the original spam images, and ROC curves of the attacked classifiers. Through further statistical analysis, the Universal Perturbation was chosen as a base for our proposed image transformation attack, due to its versatility and overall high performance in terms of accuracy reduction and computation time.

To maximize the number and intensity of natural features in an attack, the approach introduced in [15] for maximizing activations of certain layers in a deep neural network was used. This technique serves to generate sets of “natural perturbations” from the non-spam subsets of the image spam datasets. These natural perturbations were then modified via the class activation maps of all spam images in both datasets. The class activations were generated using GradCAM from the two convolutional neural networks trained on the ISH and MD datasets. These activation maps allow the regions in spam images recognized to contribute most to the spam classification to benefit from a universal adversarial perturbation.

Our technique resulted in comparable—if not greater—accuracy reduction as compared to C&W’s Attack. In addition, our approach is computation much more efficient than C&W’s Attack. Furthermore, the nature of our attack implies that the only potential computational bottleneck is generating the modified natural perturbations. This aspect of the attack would not be an issue in practice, unless a spammer generates vast numbers (i.e., in the millions) of modified adversarial spam images.

A dataset of modified adversarial spam images has been generated by the authors by applying the proposed attack to the spam subsets of the ISH and MD datasets. This dataset will be made freely available to researchers.

Future work will include evaluating the ability of adversarial attack defense methods. We will consider defensive distillation against adversarial spam images generated with our proposed attack. The goal of this research will be to develop defenses specifically designed for natural perturbation-augmented adversarial spam images. For example, the subtraction of predicted adversarial perturbations is one path that we intend to pursue.

References

- [1] Fan Aiwan and Yang Zhaofeng. Image spam filtering using convolutional neural networks. *Personal and Ubiquitous Computing*, 22(5-6):1029–1037, 2018.
- [2] Annapurna Annadatha and Mark Stamp. Image spam analysis and detection. *Journal of Computer Virology and Hacking Techniques*, 14(1):39–52, 2016.
- [3] Apache. SpamAssassin. <https://spamassassin.apache.org/>.
- [4] Campaign Monitor. Email Usage Statistics in 2019, 2019. <https://www.campaignmonitor.com/blog/email-marketing/2019/07/email-usage-statistics-in-2019/>.
- [5] Nicholas Carlini and David Wagner. Towards evaluating the robustness of neural networks. In *2017 IEEE Symposium on Security and Privacy (SP)*, pages 39–57. IEEE, 2017.
- [6] Aneri Chavda, Katerina Potika, Fabio Di Troia, and Mark Stamp. Support vector machines for image spam analysis. *Proceedings of the 15th International Joint Conference on e-Business and Telecommunications*, 2018.
- [7] Pin-Yu Chen, Huan Zhang, Yash Sharma, Jinfeng Yi, and Cho-Jui Hsieh. Zoo: Zeroth order optimization based black-box attacks to deep neural networks without training substitute models. In *Proceedings of the 10th ACM Workshop on Artificial Intelligence and Security*, pages 15–26, 2017.
- [8] Emmanuel Gbenga Dada, Joseph Stephen Bassi, Haruna Chiroma, Shafii Muhammad Abdulhamid, Adebayo Olusola Adetunmbi, and Opeyemi Emmanuel Ajibuwa. Machine learning for email spam filtering: review, approaches and open research problems. *Helijon*, 5(6), 2019.

- [9] Yan Gao, Ming Yang, Xiaonan Zhao, Bryan Pardo, Ying Wu, Thrasylvoulos N. Pappas, and Alok Choudhary. Image spam hunter. *2008 IEEE International Conference on Acoustics, Speech and Signal Processing*, 2008.
- [10] Ian J Goodfellow, Jonathon Shlens, and Christian Szegedy. Explaining and harnessing adversarial examples. *arXiv preprint arXiv:1412.6572*, 2014.
- [11] Jianguo Jiang, Boquan Li, Min Yu, Chao Liu, Weiqing Huang, Lejun Fan, and Jianfeng Xia. Restoration as a defense against adversarial perturbations for spam image detection. In *International Conference on Artificial Neural Networks*, pages 711–723. Springer, 2019.
- [12] Amara Dinesh Kumar, Soman KP, et al. Deepimagespam: Deep learning based image spam detection. *arXiv preprint arXiv:1810.03977*, 2018.
- [13] Seyed-Mohsen Moosavi-Dezfooli, Alhussein Fawzi, Omar Fawzi, and Pascal Frossard. Universal adversarial perturbations. In *Proceedings of the IEEE conference on computer vision and pattern recognition*, pages 1765–1773, 2017.
- [14] Seyed-Mohsen Moosavi-Dezfooli, Alhussein Fawzi, and Pascal Frossard. Deepfool: a simple and accurate method to fool deep neural networks. In *Proceedings of the IEEE conference on computer vision and pattern recognition*, pages 2574–2582, 2016.
- [15] Alexander Mordvintsev, Christopher Olah, and Mike Tyka. Inceptionism: Going deeper into neural networks. <https://research.googleblog.com/2015/06/inceptionism-going-deeper-into-neural.html>, 2015.
- [16] Maria-Irina Nicolae, Mathieu Sinn, Minh Ngoc Tran, Beat Buesser, Amrbrish Rawat, Martin Wistuba, Valentina Zantedeschi, Nathalie Baracaldo, Bryant Chen, Heiko Ludwig, Ian Molloy, and Ben Edwards. Adversarial robustness toolbox v1.2.0. *CoRR*, 1807.01069, 2018.
- [17] NumPy, 2020. <https://numpy.org/>.
- [18] OpenCV, 2020. <https://opencv.org/>.
- [19] Nicolas Papernot, Patrick McDaniel, Ian Goodfellow, Somesh Jha, Z Berkay Celik, and Ananthram Swami. Practical black-box attacks against machine learning. In *Proceedings of the 2017 ACM on Asia conference on computer and communications security*, pages 506–519, 2017.
- [20] Adrian Rosebrock. Zero Parameter Automatic Canny Edge Detection, 2020. <https://pyimagesearch.com/2015/04/06/zero-parameter-automatic-canny-edge-detection-with-python-and-opencv/>.
- [21] scikit-learn. Machine learning in Python, 2020. <https://scikit-learn.org/>.
- [22] SciPy, 2020. <https://scipy.org/>.
- [23] Ramprasaath R Selvaraju, Michael Cogswell, Abhishek Das, Ramakrishna Vedantam, Devi Parikh, and Dhruv Batra. Grad-cam: Visual explanations from deep networks via gradient-based localization. In *Proceedings of the IEEE international conference on computer vision*, pages 618–626, 2017.
- [24] Tazmina Sharmin, Fabio Di Troia, Katerina Potika, and Mark Stamp. Convolutional neural networks for image spam detection. *Information Security Journal: A Global Perspective*, 29(3):103–117, 2020.
- [25] M. Soranamageswari and C. Meena. Statistical feature extraction for classification of image spam using artificial neural networks. *2010 Second International Conference on Machine Learning and Computing*, 2010.
- [26] Christian Szegedy, Wojciech Zaremba, Ilya Sutskever, Joan Bruna, Dumitru Erhan, Ian Goodfellow, and Rob Fergus. Intriguing properties of neural networks. *arXiv preprint arXiv:1312.6199*, 2013.
- [27] TensorFlow, 2020. <https://tensorflow.org/>.
- [28] Xiaoyong Yuan, Pan He, Qile Zhu, and Xiaolin Li. Adversarial examples: Attacks and defenses for deep learning. *IEEE transactions on neural networks and learning systems*, 30(9):2805–2824, 2019.